Abdominal Radiology

Published online: 24 August 2018

Abdom Radiol (2019) 44:406–421
https://doi.org/10.1007/s00261-018-1741-7

Role of dual energy CT to improve diagnosis of non-traumatic abdominal vascular emergencies

Khalid W. Shaqdan,[1] Anushri Parakh,[1] Avinash R. Kambadakone,[1] and Dushyant V. Sahani[1]

[1]Department of Radiology, Massachusetts General Hospital, Harvard Medical School, 55 Fruit Street, White Building, Room 270, Boston, MA 02114, USA

Abstract

Computed tomography angiography (CTA) is the modality of choice to evaluate abdominal vascular emergencies (AVE). CTA protocols are often complex and require acquisition of multiple phases to enable a variety of diagnosis such as acute bleeding, pseudoaneurysms, bowel ischemia, and dissection. With single energy CT (SECT), differentiating between calcium, coagulated blood, and contrast agents can be challenging based on their attenuation, especially when in small quantity or present as a mixture. With dual-energy CT (DECT), virtual monoenergetic (VM) and material decomposition (MD) image reconstructions enable more robust tissue characterization, improve contrast-enhancement, and reduce beam hardening artifacts. This article will demonstrate how radiologists can utilize DECT for various clinical scenarios in assessment of non-traumatic AVE.

Key words: Dual-energy CT—Abdominal vascular emergencies—Virtual monoenergetic images—Material decomposition images

Abdominal vascular emergencies (AVE) can be life-threatening with significant morbidity and high mortality [1]. Causes of non-traumatic AVE are either due to vascular compromise or organ-related injuries. Medical conditions that fit the criteria for an emergency include acute bleeding, pseudoaneurysms, bowel ischemia, dissection, and arterio-venous malformations among others. Due to the risk of potential hemodynamic instability and end organ damage, rapid evaluation is vital for better outcome [1]. This requires a multidisciplinary approach and imaging plays an integral role in diagnosis.

Conventional computed tomography angiography (CTA) has become the standard of care in the radiologic evaluation of AVE because of its availability, rapid acquisition time, and superior image quality [2]. However, CTA protocols are complex due to multiphasic acquisitions and ensuring correct bolus timing of intravenous contrast for adequate contrast-enhancement [3, 4]. Furthermore, challenges with SECT such as limited tissue characterization and presence of image artifacts can lower diagnostic confidence and lead to repeat exams with additional used of contrast media [5, 6]. Such workflow constraints increase image interpretation time in the emergency department (ED) where rapid assessment is critical to ensure the best patient outcomes [7]. Moreover, identifying the various imaging presentations of AVE can be challenging for the ED radiologist who are not highly subspecialized [8].

Utilizing benefits of newer technologies such as dual-energy CT (DECT) can facilitate image interpretation for detecting abdominal pathologies [9]. With DECT, utilizing material optimized images and post-processing techniques can salvage suboptimal exams while simplifying complex protocols [10]. Image reconstructions such as virtual monoenergetic (VM) and material density (MD) applications enhance contrast attenuation, improve lesion conspicuity and reduce image artifacts for enhanced interpretation [11, 12]. Additionally, the potential to decrease contrast load with DECT is advantageous in vascular imaging where patients have comorbidities that put them at high risk for developing adverse effects from contrast agents (13). The ability to maintain diagnostic contrast-enhancement, despite low contrast doses, allows for compensation in suboptimal contrast-enhanced exams due to errors in bolus timing or

Correspondence to: Dushyant V. Sahani; *email:* dsahani@mgh.harvard.edu

Table 1. DECT examination protocols at our institution

rsDECT			dsDECT	
Discovery CT750 HD (GE healthcare, Milwaukee, WI)			Somatom Definition Force (Siemens Medical, Erlangen, Germany)	
Protocol	Aorta	Mesenteric ischemia	Aorta	Mesenteric ischemia
Tube voltage	80/140 kVp		100/Sn150 kVp	
Tube current (mA)	640	600	QRM 170/85	QRM 220/110
Detector	64 × 0.625		128 × 0.6	
Pitch	1.5	0.98	0.6	1
Tube rotation	0.6 s	0.8 s	0.5 s	
Slice thickness	2.5 mm		2 mm	5 mm
Iterative reconstruction	ASIR 50%		Admire level 3	
For patients < 250 lbs				

Table shows examination protocols at our institution for arterial phase
rsDECT, as rapid switching dual energy CT; dsDECT, as dual source dual energy CT; QRM, as quality reference mA; GSI, as gemstone spectral imaging; ASIR, as adaptive statistical iterative reconstruction; ADMIRE, as advanced modeled iterative reconstruction

in instances of extravasation and other patient related factors [13].Several studies have been published supporting the use of DECT throughout the body for improving diagnostic confidence [14–16]. However, knowledge of DECT applications for the assessment of emergent intra-abdominal vascular processes is limited. In this article, we will demonstrate how DECT applications aid in the detection and characterization of various clinical scenarios in non-traumatic AVE.

CT Technology and examination protocol

SECT utilizes one X-ray source that creates a polyenergetic beam with a single predetermined peak voltage [17]. Tissues are differentiated based on a precise and well-defined formula to create a scale of Hounsfield units (HU) [17]. However, SECT only provides information for X-ray linear attenuation coefficients at a single given energy and tissues with similar HU cannot be differentiated [17]. Newer generation scanners with dual-energy capability, also referred to as spectral CT or multi-energetic CT, provide additional tissue characterization capabilities. With DECT, there is enhanced discrimination of tissues as the photoelectric effect causes different tissues to have varying X-ray attenuation at different energies [12].

There are different ways of obtaining dual-energy or spectral information in CT. Dual-source DECT (dsDECT, Siemens healthcare) acquires images using two X-ray tubes which operate at different tube voltages, with additional tube filtration for larger spectral separation [12]. Single-source twin beam DECT (tbDECT, Siemens healthcare) acquires images using a single 120-kVp X-ray beam split into high-and low-energy spectra by gold and tin filters [18]. Single-source rapid kilovoltage switching DECT (rsDECT, GE healthcare) acquires images using a single X-ray tube alternating between 80 and 140 kVp [12]. Detector-based spectral computed tomography (dlDECT, Phillips healthcare) simultaneously collects low- and high-energy data with a layered detector system [12].

CT protocol with arterial and portal venous phases is the standard of practice when evaluating for AVE. At our institution, CTA protocols are biphasic with arterial phase acquired using dual-energy. For abdominal CTA studies, we administer between 60 and 90 mL (based on body weight) of iodinated contrast material (370 mgI/mL). DECT angiography protocols for both rsDECT and dsDECT at our institution are demonstrated in Table 1.

DECT image post-processing

Advanced processing with DECT occurs after image acquisition to generate VM and MD images [11]. Any desired single-photon energy (monoenergetic) level between 40 and 200 keV can be generated depending on the platform. A two- or three-material decomposition (iodine, fat, soft tissue) algorithm is applied to generate virtual unenhanced (VUE) and MD images [11]. VM and MD images enhance contrast attenuation, improve lesion conspicuity, and reduce image artifacts to overcome image quality limitations of SECT [11]. Low-energy VM images (40–55 keV) display increased contrast attenuation, intermediate-energy (60–75 keV) have optimal peak contrast-to-noise ratio equivalent to SECT images (120 kVp), and high-energy (95–200 keV) images are used for suppressing metal related artifacts [11]. VM images also provide more consistent measurements between CT attenuation numbers and iodine concentrations under beam hardening conditions improving lesion detection [19, 20].

DECT is capable of acquiring the electron density and effective atomic number for different materials in a quantitative manner [21]. Materials such as iodine and calcium can be separated based on their attenuation profiles at different energies to create novel image

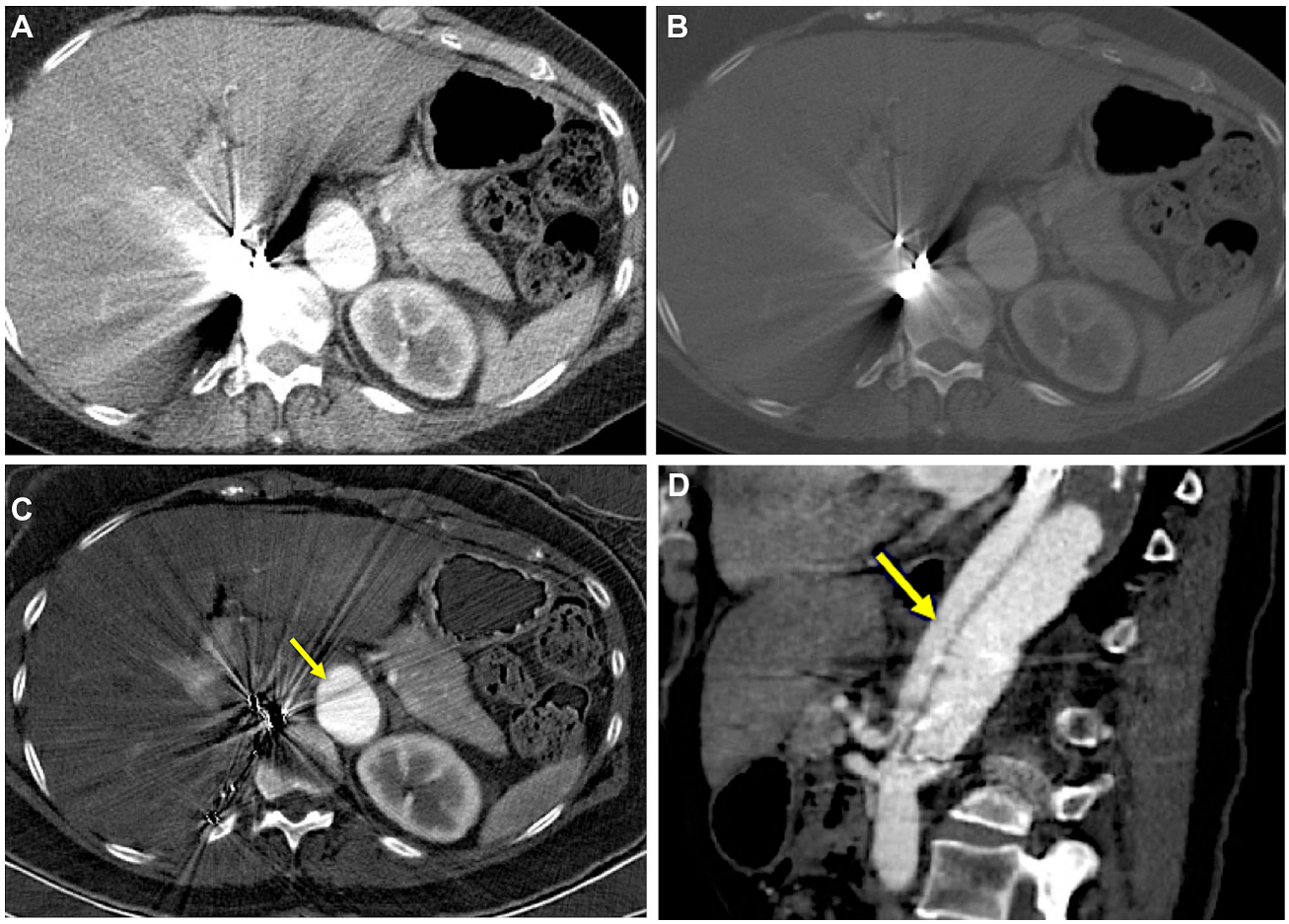

Fig. 1. Reduction of artifacts. 59 year old female with interscapular pain (rsDECT 80/140 kVp). 50 keV VM image in abdominal (**A**) and bone (**B**) windows are of limited diagnostic quality for the caudal extent of dissection flap due to presence of surgical clips artifacts. MD-I image (**C**) suppresses the artifacts revealing a dissection flap (arrow). Sagittal reconstruction (**D**) confirms the caudal extent.

reconstructions [22]. MD iodine (MD-I) images, which are based on iodine and water attenuations, are routinely used for diagnostic workup and can be reconstructed on all commercially available DECT vendors with generally good agreement in iodine quantification [23]. MD-I images help discriminate contrast from other materials and allow for effective reduction of artifacts from metals with high atomic number (e.g., embolization coils with platinum) (Fig. 1) [22]. MD-I images are independent of inherent tissue attenuation allowing for a more accurate and objective measurement of enhancement compared to HU that is derived from SECT [22]. VUE images can be generated from contrast-enhanced DECT scans replacing the need for TUE phase significantly reducing radiation dose [24, 25]. MD calcium images can be reconstructed to isolate or remove calcium within the vessel lumen for better stenosis assessment [22].

Clinical application of DECT in non-traumatic AVE

Vascular compromise

Stenosis assessment and plaque characterization

Assessing degree of vascular stenosis is important to determine risk of end organ injury. Additionally, distinguishing calcified from non-calcified plaques is helpful to identify unstable soft plaques that may lead to an embolic event.

On CT, vascular stenosis is observed as narrowing of the vessel lumen [26]. However, blooming artifacts caused by beam hardening from heavily calcified plaques make it challenging to assess luminal stenosis and differentiate the plaque from iodine on SECT [27]. With DECT, subtraction of calcium on MD images makes it feasible to determine true lumen versus pseudo-filling

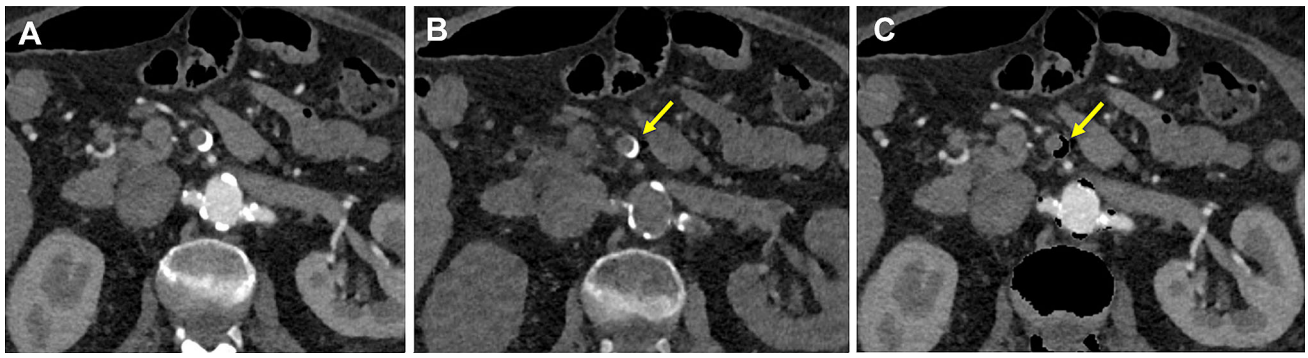

Fig. 2. Differentiating iodine versus calcium. 72 year-old female with postprandial abdominal pain (dsDECT 80/Sn140 kVp). SECT-equivalent axial (**A**) image shows a peripheral crescentic hyperattenuation in the proximal superior mesenteric artery (SMA) (arrow). VUE (**B**) and selective calcium-subtraction (**C**) images suggests the hyperattenuation as a calcified plaque with no iodine within the vessel lumen, confirming the diagnosis of SMA thrombosis. Also note improved delineation of the bilateral renal plaques versus the contrast opacified patent lumen.

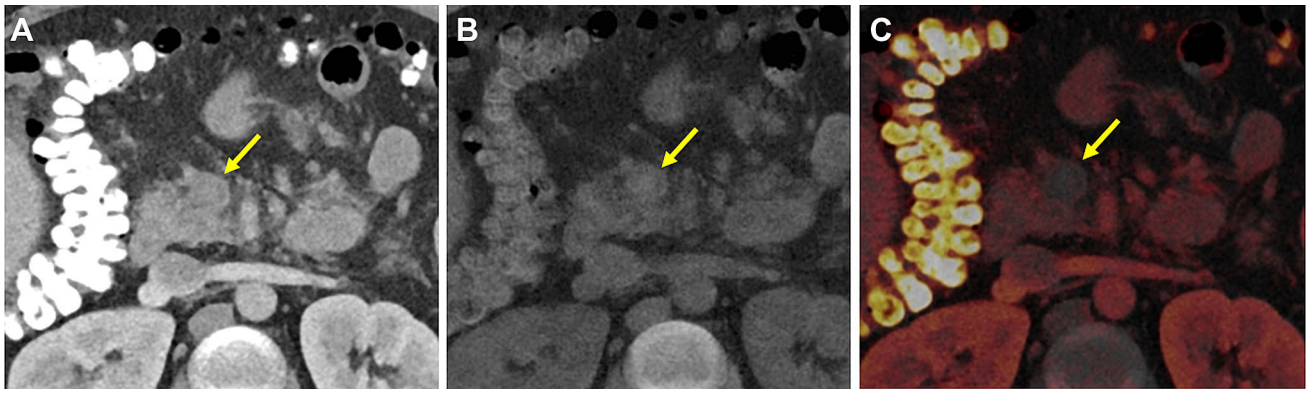

Fig. 3. Improving thrombus conspicuity. 55 year old male with a history of chronic portal vein thrombosis presents with worsening abdominal pain (dsDECT 100/Sn150 kVp). SECT-equivalent (**A**) image shows interval development of a filling defect within the expanded superior mesenteric vein. VUE (**B**) image reveals hyperdense clot in the SMV suggesting acute extension of a bland thrombus. MD-I color overlay (**C**) images confirm no uptake or enhancement of the superior mesenteric vein.

defects as a result of contrast media mixing with non-opacified blood (Fig. 2).

Venous thrombosis and characterization

Abdominal venous occlusion includes thrombosis of the mesenteric, portal, and hepatic veins among others. Mesenteric venous thrombosis (MVT) accounts for 1 in 1000 emergency surgical laparotomies for acute abdomen [28]. Acute MVT is typically caused by new-onset thrombosis of the superior mesenteric vein (95% of cases) [29]. Malignancy is present in up to 16% of acute MVT cases [29]. On SECT, bland thrombus typically appears hypodense in the affected vein. With DECT, MD-I images minimize soft tissue signal enhancing the contrast between opacified vessels and thrombi thereby improving conspicuity of thrombi (Fig. 3). Moreover, MD-I images can be used to distinguish bland thrombus from tumor thrombus regardless of the extent of arterial enhancement or size of affected vessels (Fig. 4) [29]. Ascenti et al. reported significantly higher diagnostic accuracy using iodine quantification (97%) compared to conventional enhancement measurements (88.2%) in characterization of portal vein thrombus in the setting of hepatocellular carcinoma (HCC) [29].

Dissection

Dissections are caused by tears on the inner linings of vessels and can progress through the entire wall leading to rupture. The aorta is the most common site of dissection with an incidence of 2000 cases per year in the United States [30]. Rapid diagnosis of aortic dissection is

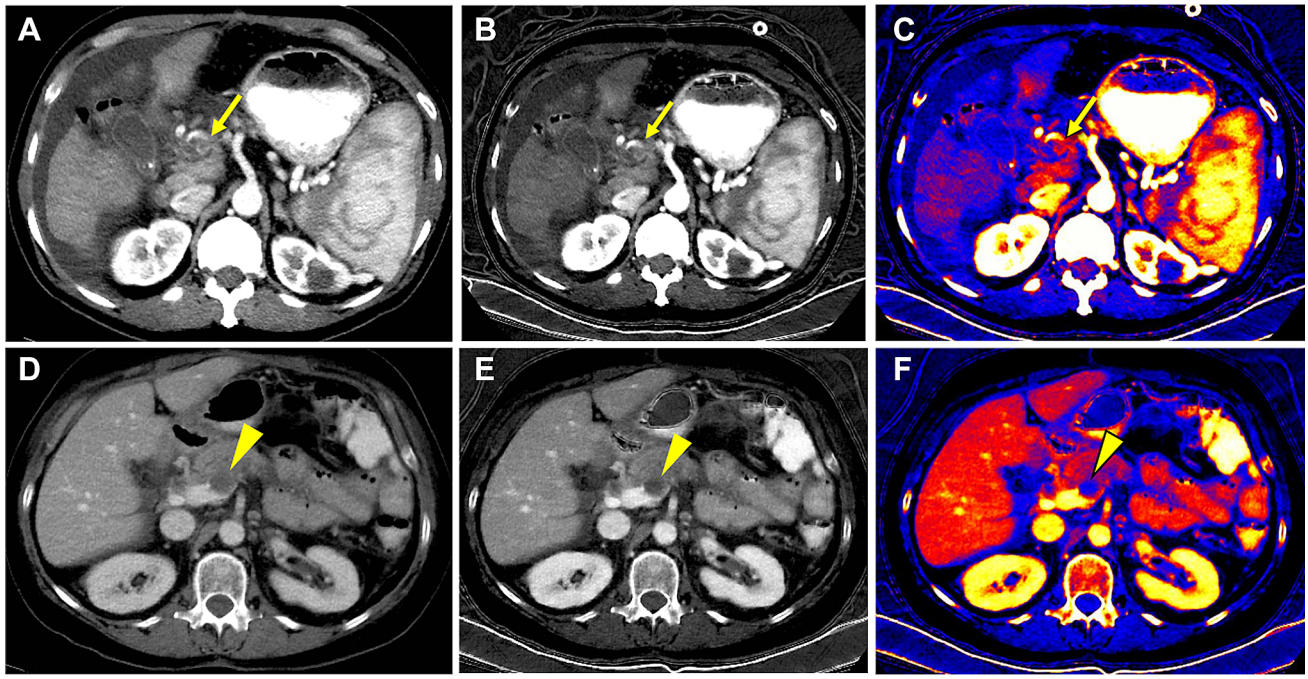

Fig. 4. Tumor characterization. Portal vein thrombus in two different patients (rsDECT 80/140 kVp). 65 keV VM (**A**), MD-I (**B**) and color overlay (**C**) images show tumor thrombus (arrows) in a patient with HCC. 65 keV VM (**C**), MD-I (**D**) and color overlay (**E**) images show bland thrombus (arrowhead) in a patient with ovarian cancer. MD-I images help detect subtle enhancement in the tumor thrombus.

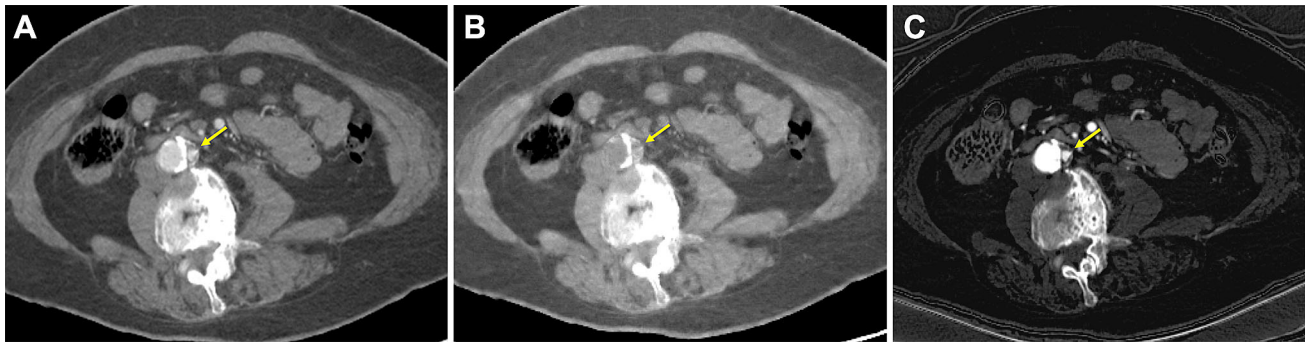

Fig. 5. Increased conspicuity of focal dissection. 82-year-old female presents with abdominal pain (rsDECT 80/140 kVp). 50 keV VM (**A**) image shows focal partially thrombosed dissection involving the distal aorta. VUE (**B**) shows the presence of calcifications along the wall, while the axial (**C**) image demonstrates the focal dissection more conspicuously.

critical due to high mortality rates [30]. With DECT, low keV VM and MD-I images provide higher contrast-enhancement and superior image quality for aorto-illiac evaluation compared to SECT [31]. Additionally, VM and MD-I images can expose areas of aortic pathology obscured by image artifacts on SECT. Infrequently, dissection of the mesenteric arteries may also occur in conjunction with aortic dissection or in isolation due to iatrogenic causes or spontaneously [32]. MD-I and lower energy VM images can illustrate such isolated dissections with more conspicuity (Fig. 5).

Vascular leaks

Pseudoaneurysm

Abdominal visceral artery pseudoaneurysms typically result from trauma, inflammatory processes, or iatrogenic causes (e.g., post-biopsy) [33]. The most commonly involved vessel is the splenic artery with rarer occurrence in the celiac or mesenteric vessels [33]. Complications include early rupture, mass effect on adjacent structures, and infection [33]. On CT, visceral artery pseudoanuerysms appear as round or oval outpouchings

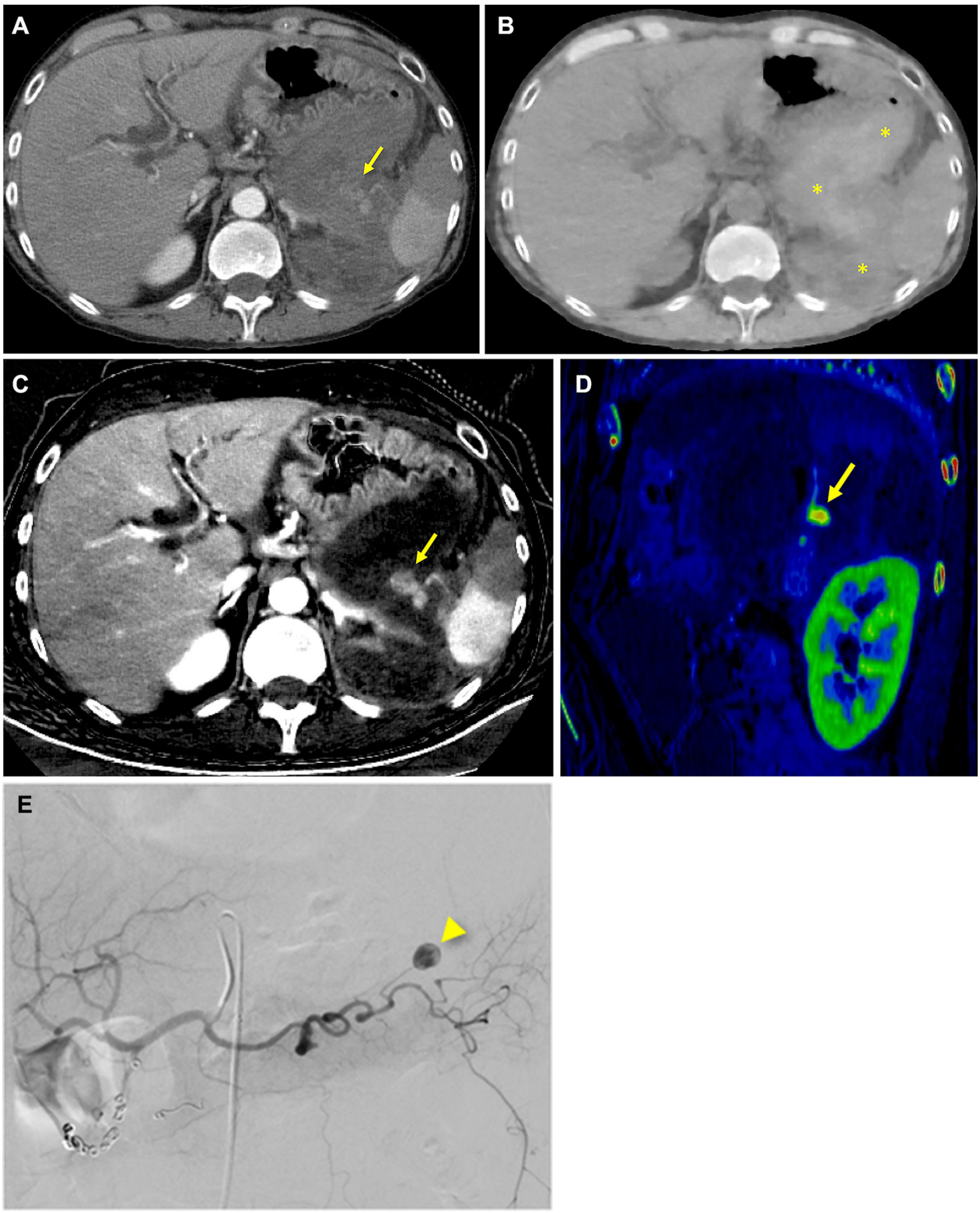

Fig. 6. Splenic artery pseudoanuersym. 53-year-old male with chronic pancreatitis and acute episode of abdominal pain (rsDECT 80/140 kVp). 65 keV VM image (**A**) shows a heterogeneous collection in the left upper quadrant with a subtle hyperattenuating focus (arrow). VUE image (**B**) reveals hyperdense areas (asterisks) confirming the presence of blood products. Axial (**C**) and color overlay sagittal (**D**) MD-I images show improved delineation of the saccular pseudoaneurysm arising from the splenic artery. Angiogram (**E**) confirmed diagnosis of splenic artery pseudoanuersym (arrowhead) and patient was managed by embolization.

Fig. 7. Endoleak detection. 65 year old female post EVAR and endoleak embolization (rsDECT 80/140 kVp). 50 keV VM (**A**) image shows an enhancing area in the posterior aspect of the sac (persistent endoleak) which was obscured by artifacts from onyx on conventional SECT images (**B**). MD-I image (**C**) suppresses the artifacts while demonstrating a leak without ambiguity.

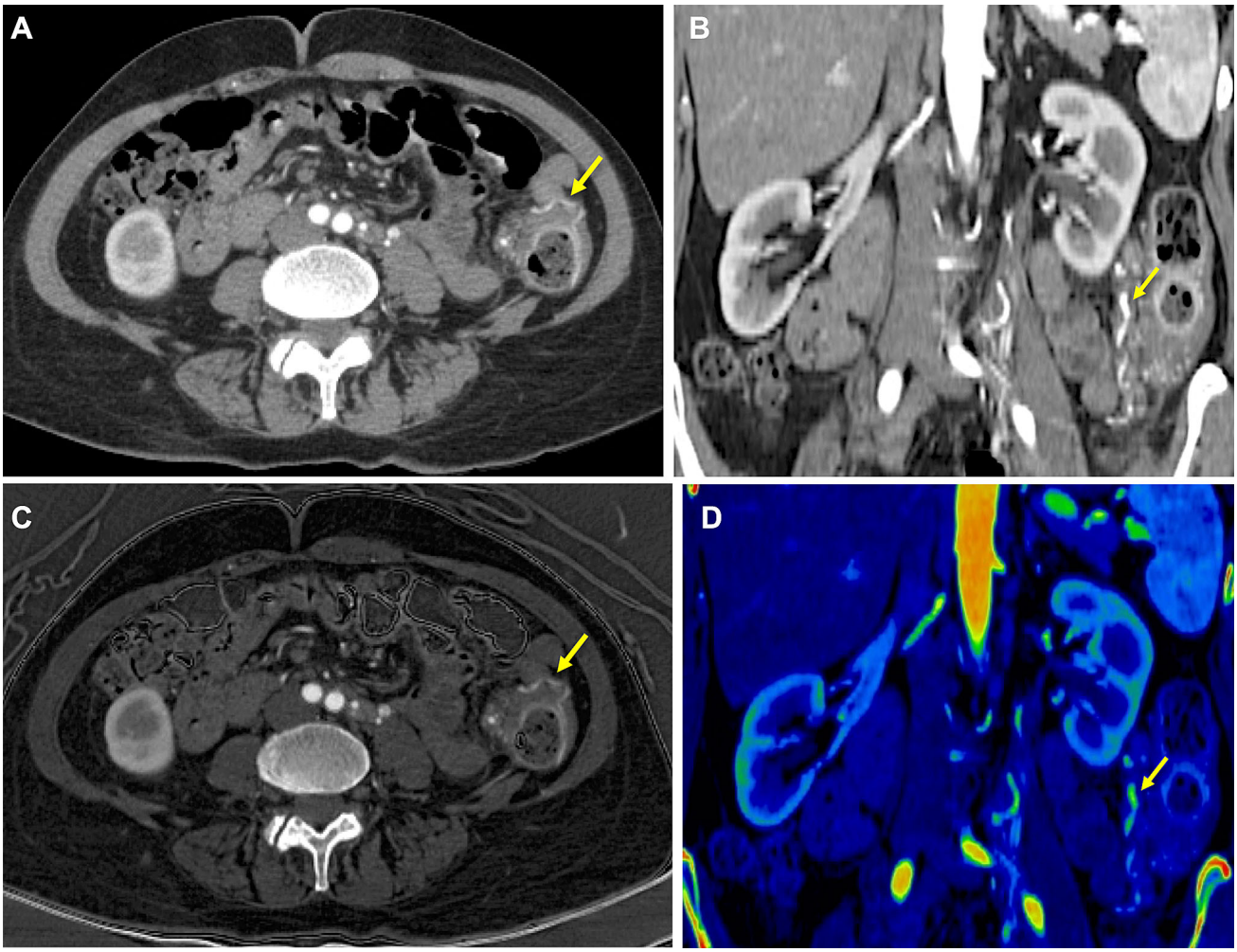

Fig. 8. Colonic arterio-venous malformation. 50-year-old male with history of a pulsatile abdominal mass (rsDECT 80/140 kVp). 50 keV VM (**A**, **B**) image shows diffuse circumferential thickening of the descending colon. Axial (**C**) and color overlay coronal MD-I (**D**) images show increased conspicuity of the tortuous vessels along the serosal surface of the thickened bowel loop (arrows).

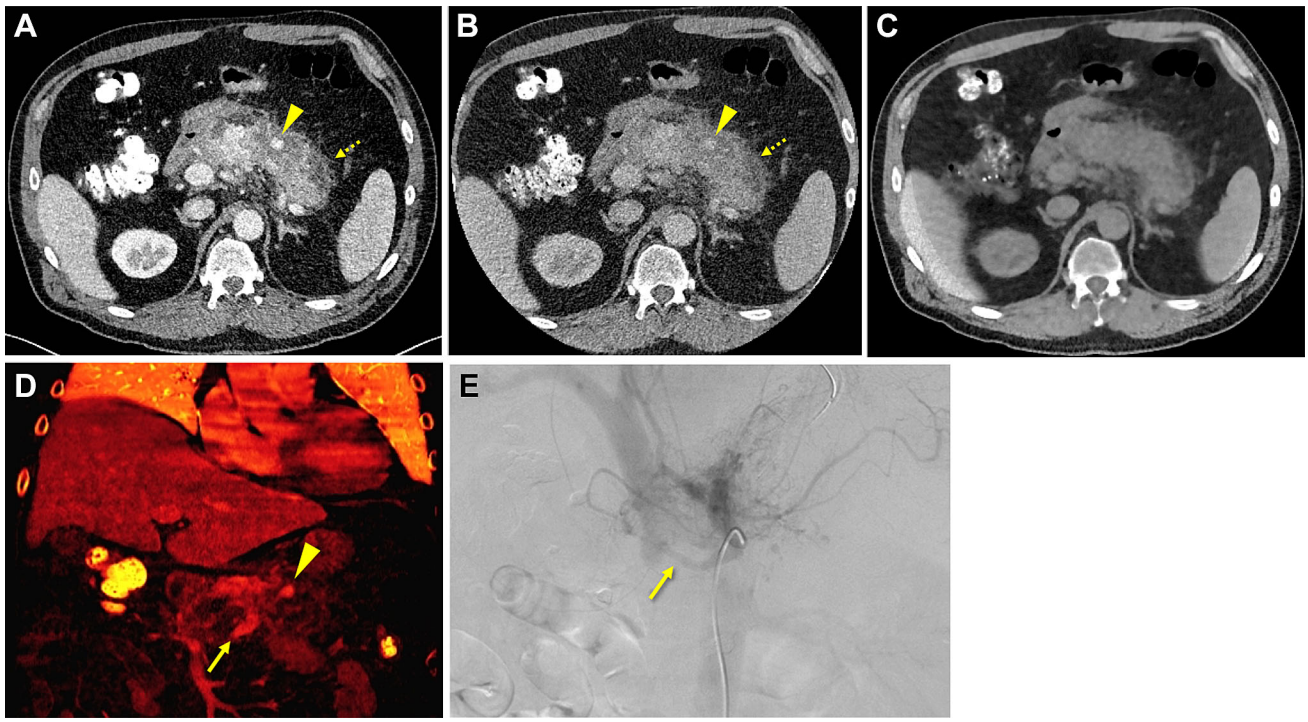

Fig. 9. Pancreatic vascular pathologies. 54-year-old male with necrotizing pancreatitis and worsening epigastric pain (dsDECT 100/Sn140 kVp). 100 kVp (**A**) and 140 kVp (**B**) images show diffuse heterogeneous enhancement of the pancreas (interrupted arrows) with areas of necrosis and a focal hyperenhancing area within the pancreatic body (pseudoaneurysm; arrowhead). Though 100 kVp image delineates the pathology better compared to 140 kVp image in this 104 kg patient, the image has high noise. No hemorrhagic areas are noted on VUE (**C**). Coronal MD-I (**D**) image accentuates visualization of necrotic and pseudoaneurysm by suppressing the soft tissue signal. A draining vein (arrow) was also conspicuous on MD-I that was confirmed as an AVM on conventional angiogram (**E**) and drained into the porto-splenic confluence. Patient was managed with sclerotherapy.

arising from the vessel wall with non-thrombosed portion demonstrating equal density to the intra-arterial contrast material [33]. In our collective experience with DECT, MD-I images can delineate the pseudoaneurysms better and VUE images help detect complications such as rupture. Low-energy VM images improve differentiation of hematoma from active extravasation (Fig. 6).

Although data specifically for use of DECT in assessment of pseudoaneurysms in the abdomen may be limited, there is sufficient literature where the value of using MD-I and VUE to evaluate vascular anatomy and pathology for a variety of indications has been well supported [34, 35].

Endoleak

Endoleak is a frequent complication after endovascular aneurysm repair that is usually treated with embolization. If an endoleak goes undetected, the patient can develop persistent blood loss and hemodynamic instability which can be life-threatening. With DECT, low-energy VM and MD-I images increase visualization of iodine allowing for improved conspicuity of contrast in the aneurysmal sac beyond the graft (Fig. 7). Maturen et al. demonstrated that endoleak conspicuity ratings were higher at 55 keV compared to 75 keV VM images [36]. Additionally, noise-optimized VM images at 40 keV demonstrated improved diagnostic accuracy for the detection of endoleaks compared to non-optimized VM and standard blended images [37]. MD-I can also be used to suppress image artifacts caused by embolization coils to enable better evaluation of residual endoleaks (Fig. 7). Furthermore, a single phase examination with DECT by generating VUE has shown comparable diagnostic performance for endoleak detection compared to bi- or tri-phasic SECT protocol with up to 61% radiation dose reduction [38–41].

Arterio-venous malformations

Arterio-venous malformations (AVMs) consist of abnormal connections between arteries and veins which are an important vascular cause of lower GI bleeding [42]. AVMs are relatively common in the cecum or right colon, with a much lower incidence in other areas such as the pancreas (0.9%) [43, 44]. DECT images have proven effective for early detection of AVMs in other areas of the body and the same techniques can be used to improve diagnosis in the abdomen [45–47]. Low-energy VM and

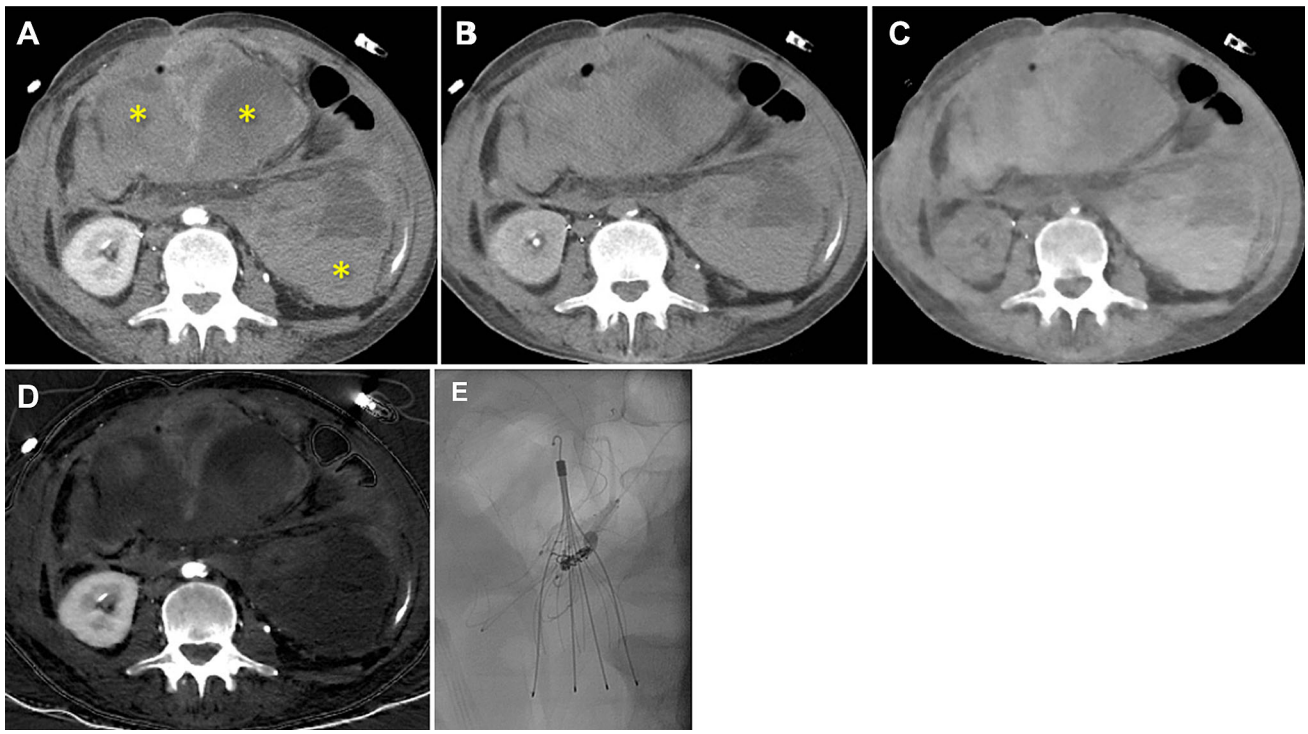

Fig. 10. Hemoperitoneum. 33-year-old male with a history of duodenal ulcer presents with generalized abdominal pain (rsDECT 80/140 kVp). 65 keV VM image (**A**) shows a large intra-abdominal collection with fluid–fluid levels suggestive of intraperitoneal hemorrhage (asterisks) confirmed on TUE image (**B**). Hyperdense blood products are easily appreciated on VUE (**C**). MD-I (**D**) image shows no active extravasation at the time of the scan. Angiogram (**E**) revealed right colic branch of SMA as the source of bleed and was subsequently embolized.

MD-I images can illustrate tortuous vessels with better conspicuity and clearly depict relationship between the AVM and surrounding structures for appropriate treatment planning (Figs. 8, 9).

Organ injury

Peritoneum

Abdominal hemorrhage is a major medical emergency with mortality rates as high as 40% [48]. On CT, active hemorrhage is demonstrated on arterial phase as a focus of high-attenuation that is not observed on TUE images [49]. With SECT, measuring attenuation values is an important method to differentiate between low-attenuation fluid, contrast, and blood [49]. However, dilute contrast agent and hemorrhage can have similar attenuation values which can delay diagnosis and subsequent management. With DECT, MD-I and VM images increase conspicuity of active bleeding, and VUE clearly depict high-attenuation hematoma (Fig. 10).

Gastrointestinal

Acute gastrointestinal (GI) bleeding can present as an emergency depending on the severity and is an important cause of morbidity and mortality [50]. GI bleeding may occur anywhere from the esophagus to the rectum. Prompt and appropriate treatment on the basis of CT findings depends on the detection of extra-luminal contrast indicating active extravasation which remains on delayed phase but not visualized on TUE scans [51]. However, hyperattenuating material in the bowel such as previously ingested metal-containing medication can be confused with vascular contrast material [52]. DECT allows accurate characterization of active GI bleeding in the bowel lumen using a dual phase protocol (arterial and venous) with comparable diagnostic performance to tri-phasic SECT (TUE, arterial, portal venous) [53]. VM and MD-I images can demonstrate the bleed with better conspicuity, and VUE can differentiate extravasation from hemorrhage (Figs. 11, 12). Additionally, MD-I images can distinguish iodine and barium (Z = 56, Z = 53; respectively) from high-density medications such as magnesium or bismuth-based drugs (Z = 12, Z = 83; respectively) (Fig. 13) [54]. However, it should be noted that there is difficulty differentiating iodine from barium on DECT images due to similarity of attenuation ratios for these agents (Fig. 14) [55].

Acute mesenteric ischemia

Acute mesenteric ischemia (AMI) is caused by sudden interruption of blood supply to the small intestine most

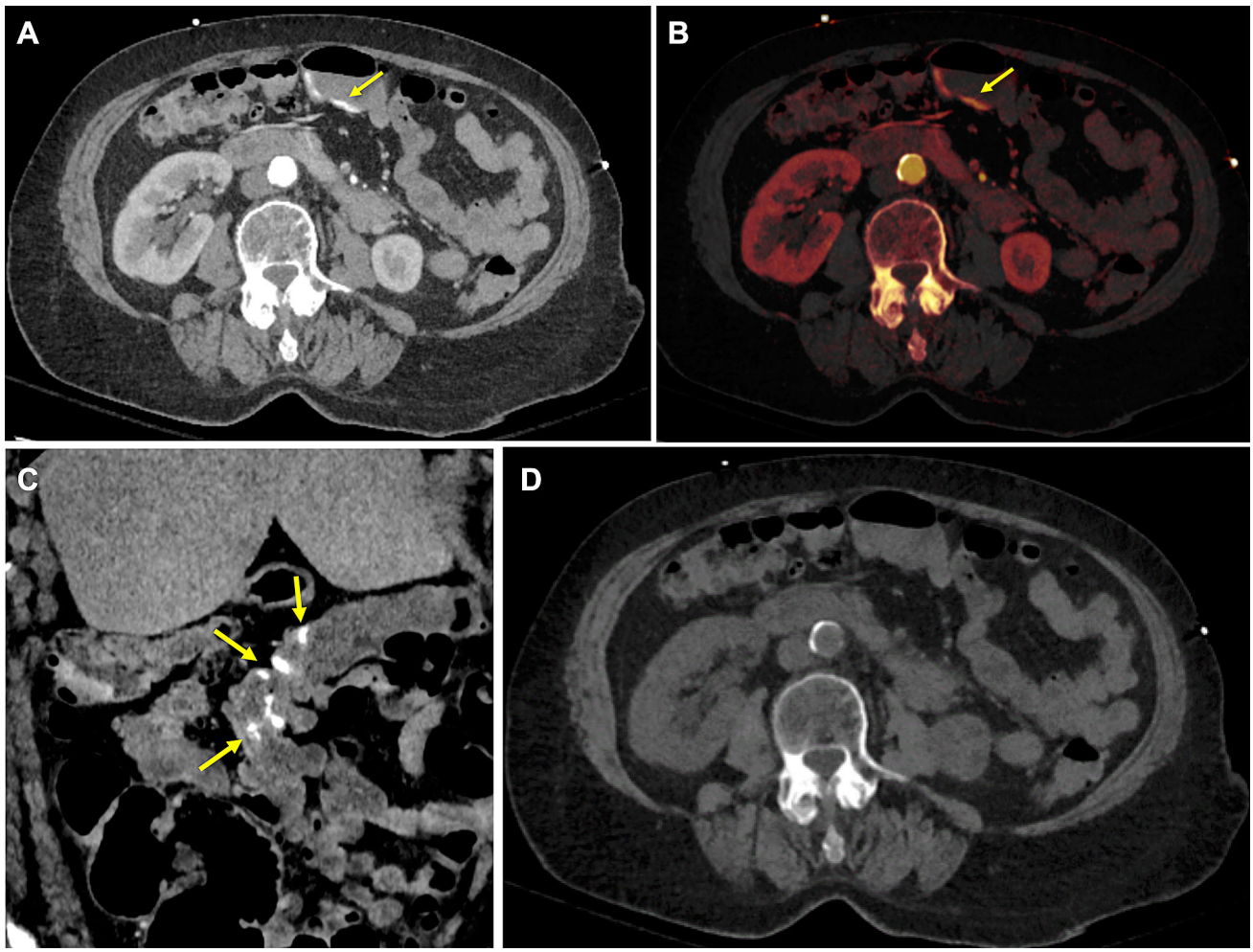

Fig. 11. Active contrast extravasation. 76-year-old female with diverticulosis and painless hematochezia (dsDECT 100/Sn150 kVp). SECT-equivalent (**A**) image shows hyperattenuating material within the transverse colon. Color overlay MD-I (**B**) and 50 keV VM (**C**) images improve conspicuity of the intraluminal contrast extravasation (arrows). VUE (**D**) image shows lack of hyperdense area in the corresponding location confirming extravasation.

commonly due to arterial occlusion (50%–70%) followed by low-flow states (20%) and venous occlusion (5%–10%) [56]. On CT, bowel ischemia appears as altered enhancement of the bowel wall or thickening in reperfusion state [56]. However, detecting an ischemic segment may be challenging as subtle differences in enhancement of a poorly perfused bowel may be hard to appreciate. With DECT, low keV VM images enhance visualization of perfused and non-perfused tissue in greater detail (Fig. 15). A study on swine models by Potretzke et al. demonstrated that VM images at 51 keV provide two-fold increase in attenuation difference between ischemic and perfused segments when compared to conventional imaging at 120 kVp [57]. Additionally, MD-I images improve conspicuity of subtle enhancement differences and enable quantitative measurements of bowel wall iodine content [58].

Liver

Spontaneous hepatic bleeding is an infrequent condition mainly caused by the rupture of an underlying hypervascular tumor [49]. In certain cases, the tumor bleed may be very subtle and undetectable on conventional SECT. With DECT, MD-I and low-energy VM images can improve evaluation of hypervascular masses by highlighting minimal enhancement in a lesion (Fig. 16).

DECT workflow and technological considerations

Technologists play an important role in deciding if DECT can be used for the patient. For dsDECT, distribution of the body weight must be taken into account as the reconstruction field-of-view (FOV) of the high-energy tube is limited to 33–35 cm [10]. Careful positioning is critical to ensure relevant anatomic structures

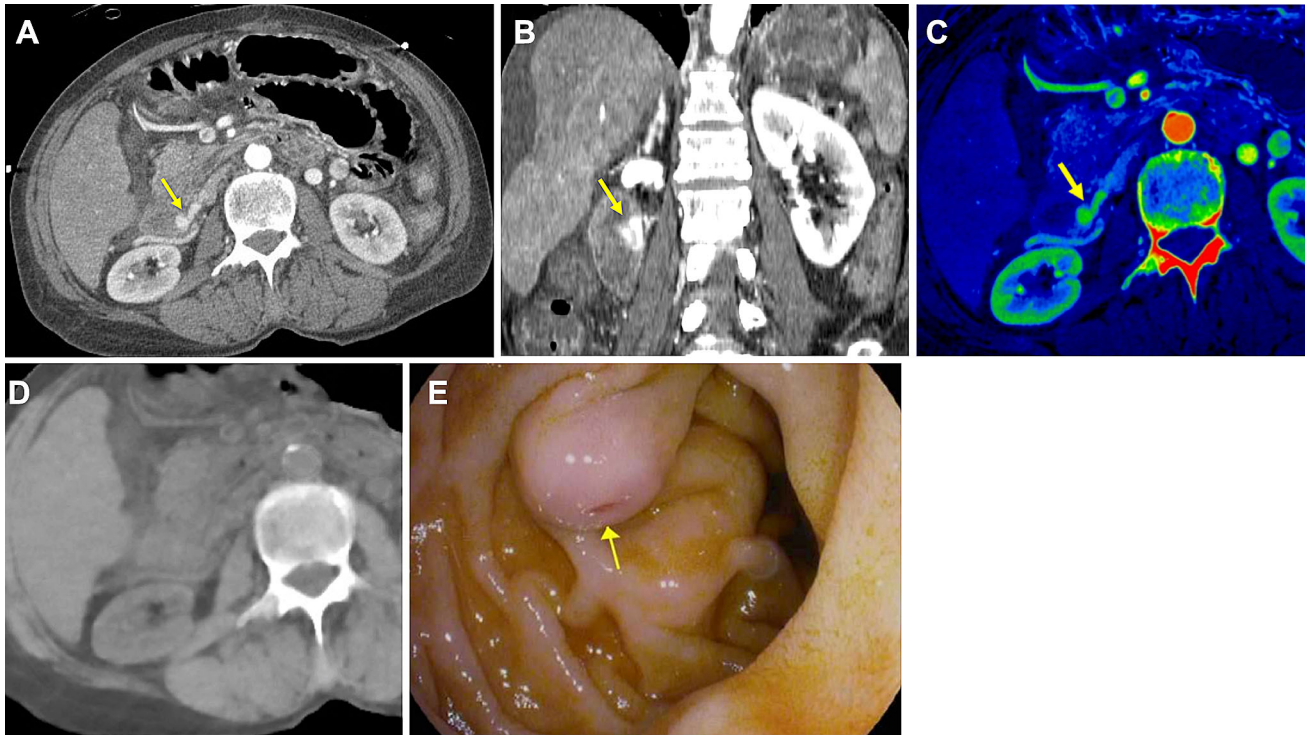

Fig. 12. Duodenal varices. 65-year-old female with a history of hepatitis C presenting with hematemesis (rsDECT 80/140 kVp). 65 keV VM (**A**) image shows hyperattenuating area within the duodenal lumen (arrow). Coronal 50 keV (**B**) and axial color overlay MD-I (**C**) images make the abnormality more discernible. VUE (**D**) image confirms absence of hyperdensity within the bowel loop. Endsocopy (**E**) confirms the presence of duodenal varices.

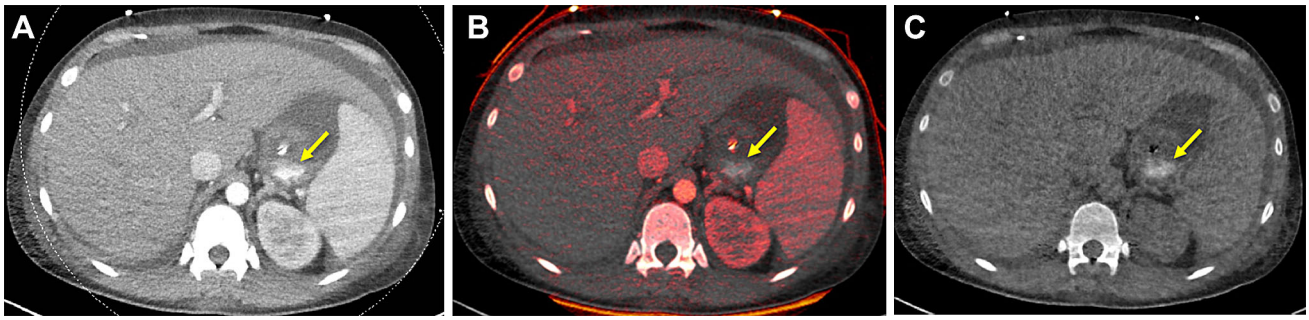

Fig. 13. Distinguishing extravasation from high attenuating medication. 31-year-old female with suspicion of gastrointestinal bleeding (dsDECT 80sn/140). SECT-equivalent (**A**) image shows hyperdense area within the gastric lumen (arrow). Color overlay MD-I (**B**) image shows no iodine uptake in the corresponding location. VUE (**C**) image shows intrinsic hyperdensity suggestive of no extravasation. Patient provided history of consuming magnesium containing medication.

are placed within the dual-energy reconstruction FOV (10). For rsDECT systems, a dual-energy FOV of 50 cm is available [10]. The lower tube potential of 80 kVp limits DE acquisition of patients who weigh more than 250 lb (113 kg) on rsDECT. Iterative reconstruction algorithms available in both dsDECT and rsDECT scanners improve image quality allowing for reduced mA acquisition, thereby reducing radiation dose [59, 60]. Newly introduced detector-based spectral CT have no limitations on gantry rotation time, field-of-view, or cross-scatter [61].

Previously, wide-spread and routine use of DECT in clinical practice was limited by high cost, increased number of images, additional training requirements, and greater operational complexity [62]. Due to increased research data leading to more implications in care,

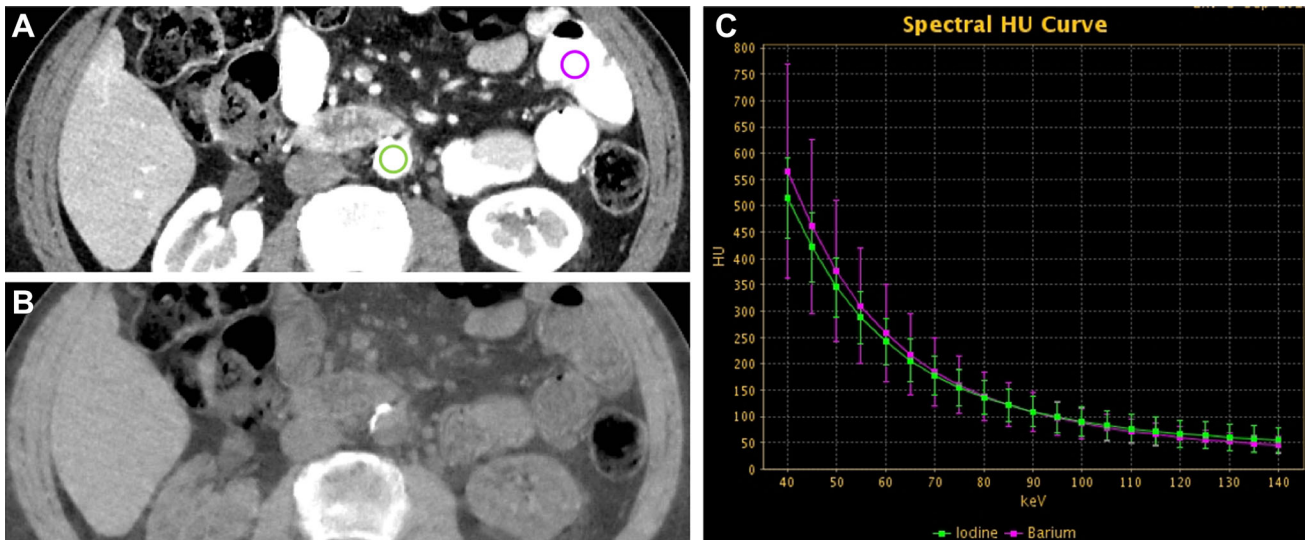

Fig. 14. Iodine and Barium on DECT. **A** Similar HU is seen for iodine (green) and barium (purple) on SECT (~ 252HU). VUE (**B**) image shows removal of both materials and spectral curve (**C**) shows similar attenuation profile across all keV levels.

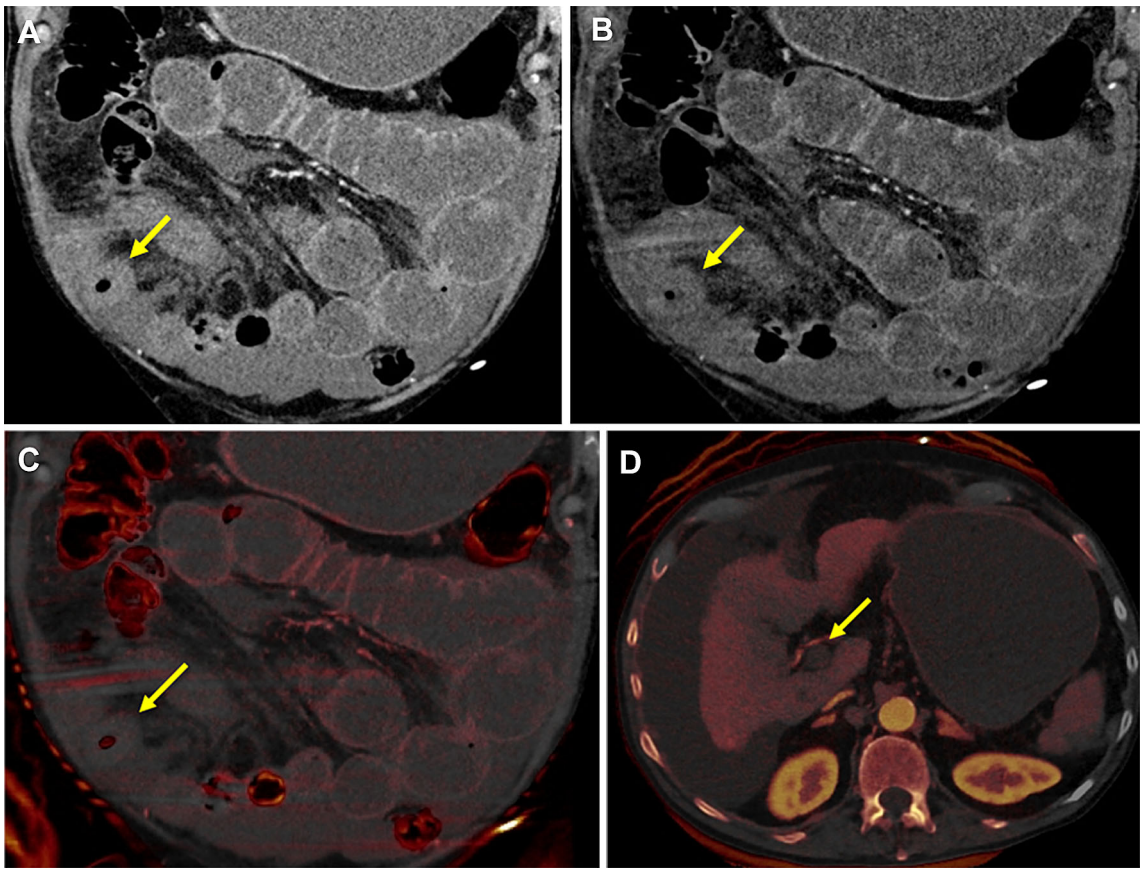

Fig. 15. Mesenteric Ischemia. 68-year-old man with liver cirrhosis presenting with postprandial abdominal pain (dsDECT 80/Sn140 kVp). SECT-equivalent (**A**) image shows thickened hypoenhancing small bowel loop (arrow). 50 keV VM (**B**) image and color overlay MD-I images (**C**) improve conspicuity of the lack of enhancement suggestive of ischemic bowel injury. Upper abdominal color overlay MD-I (**D**) image reveals bland portal vein thrombus (arrowhead).

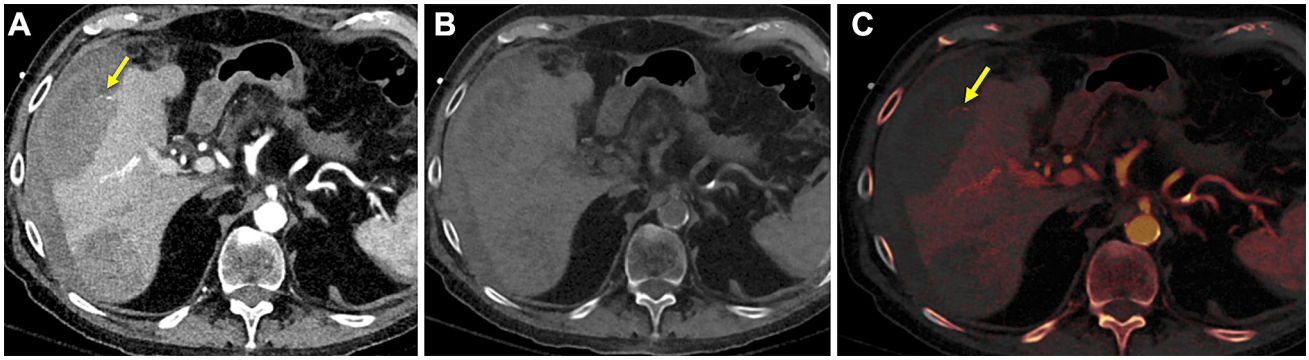

Fig. 16. Spontaneous hepatic hemorrhage. 81-year-old male presents with right-sided shoulder and abdominal pain (dsDECT 100/Sn140 kVp). 50 keV VM (**A**) image shows hypodense subcapsular lesions in the liver. VUE (**B**) image reveals hyperdense areas (arrowhead) within the collection suggesting hemorrhage. Color overlay MD-I (**C**) image shows a small hyperattenuating linear area extending into one of the lesions (arrow) suggesting active extravasation.

DECT applications have become part of standard care guidelines for a few clinical pathologies [63]. Furthermore, workflow constraints have been addressed through continued education of technologists and better post-processing automation. Appropriate technologist training and engagement is essential to effectively incorporate DECT into the clinical workflow on a regular basis [62]. Recent versions of DECT platforms and software upgrades have the capability to automate post-processing such that DECT image reconstructions do not hinder workflow [61]. For dlDECT, Spectral data are available for all patients without change in clinical workflow, allowing for improved assessment of incidental findings, artifact reduction, and dual-energy applications [61].

Contrast medium and radiation dose considerations

Contrast-enhanced CT (CECT) is integral for vascular imaging, however there are debatable concerns on the safety of iodinated IV contrast particularly in patients with vascular disease who have multiple comorbidities (diabetes, hypertension) [64]. Alternative modalities such as MR and ultrasound which may be safer for this patient population can be challenging to perform in the emergency setting, and are typically preserved for a focused approach when the cause of patient disease is already known rather than screening. Thus, CECT is the modality of choice and there remains a continued incentive to keep iodinated contrast doses at lowest levels [13]. Obtaining adequate image quality with lower iodine doses is challenging on SECT both at 120 kVp due to lower image contrast and at 100 kVp due to higher image noise. However, DECT VM spectra allow for optimal contrast visualization at low keV and artifact reduction at high keV to enable contrast medium dose reduction while maintaining diagnostic image quality (Fig. 17) [13, 65, 66]. Standard-iodine-dose for SECT typically ranges between 30 and 37 g, but with DECT a mean iodine dose as low as 15 g has been shown to be diagnostic for CTA protocols [13]. Agrawal et al. reported up to 185% higher attenuation and 25% higher contrast-to-noise ratio with low-energy VM images from reduced-iodine (24 g I) on rsDECTA of the abdomen compared to standard-iodine-dose (33.3 g I) on SECTA [66].

DECT provides several opportunities to minimize radiation dose, equivalent to or even lower than SECT, while maintaining diagnostic image quality [67, 68]. The ability to omit additional acquisitions due to higher informational content and post-processing flexibility of DECT allows for substantial radiation dose savings. The estimated radiation dose reduction by replacing TUE acquisition for VUE images is reported to range from 19% to 50% depending on the protocol [69, 70]. While omission of phases remains a way to curb radiation doses with DECT, in general various studies indicate that with newer iterative reconstruction techniques and DECT platforms the radiation doses with DECT are with conventional 120 and low (100) kVp scans [71]. Existing literature has demonstrated radiation doses ranging between 12.7 and 21.8 mGy for DECT scans of the abdomen [72–77]. These doses are well below the 25-mGy diagnostic reference levels for adult abdomen studies recommended by the American College of Radiology [78]. Moreover, DECT applications have been shown to add value for incidental lesions avoiding the need for follow-up CT exams that would otherwise increase radiation dose exposure [79]. Another potential method of radiation dose reduction with DECT is the feasibility to reduce dose of iodinated contrast media [80].

Conclusion

DECT presents a unique opportunity over SECT, with additional capabilities for problem-solving vascular imaging findings. Each clinical scenario has different diagnostic challenges and knowledge of dual-energy applications can improve reader confidence to facilitate

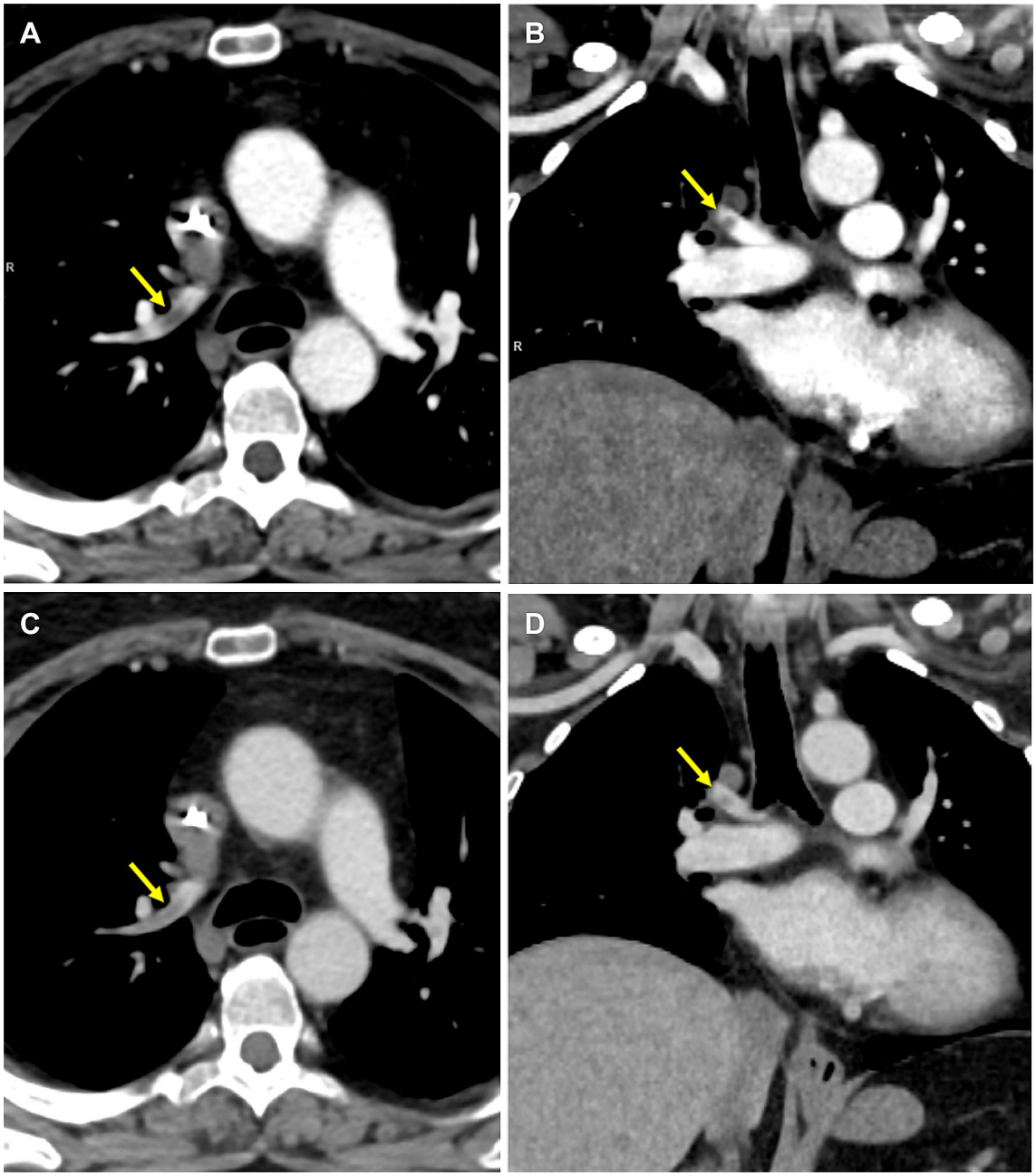

Fig. 17. Reduction of iodine dose. 54-year-old female with shortness of breath (dsDECT 100/Sn140 kVp). Patient received 36 mL intravenous iohexol (370mgI/mL) at 3 mL/sec followed by 40 ml saline flush.40 keV axial (**A**) and coronal (**B**) image reconstructions improve conspicuity of pulmonary embolus in the posterior segmental branch of right upper lobe due to increased attenuation of iodine at low keV compared to SECT-equivalent images (**C**, **D**).

clinical interpretation. Lower energy VM images increase conspicuity of iodine distribution rendering easy identification of extravasation. MD images help differentiate materials with high-attenuation values, distinguish thrombus types, permit subtraction of vessel calcification improving vessel lumen delineation, and aid in artifact suppression with preserved or increased vessel contrast. These techniques pave the way towards a more functional and quantitative assessment improving diagnostic accuracy and decreasing interpretation time while lowering contrast medium dose and radiation exposure.

Compliance with ethical standards

Funding This study was not funded.

Conflict of interest Dushyant Sahani received grant support from GE healthcare, Advisory Board of Allena Pharma, receives royalties from Elsevier publishing for textbook on Abdomen Imaging. Other authors declare that they have no conflict of interest.

Ethical approval This article does not contain any studies with human participants performed by any of the authors.

References

1. Genovese EA, Fonio P, Floridi C, et al. (2013) Abdominal vascular emergencies: US and CT assessment. Crit Ultrasound J 5(Suppl 1):S10
2. Hansen NJ (2016) Computed tomographic angiography of the abdominal aorta. Radiol Clin N Am 54(1):35–54
3. Fuentes-Orrego JM, Pinho D, Kulkarni NM, et al. (2014) New and evolving concepts in CT for abdominal vascular imaging. RadioGraphics 34(5):1363–1384
4. Kondo H, Kanematsu M, Goshima S, et al. (2010) Body size indexes for optimizing iodine dose for aortic and hepatic enhancement at multidetector CT: comparison of total body weight, lean body weight, and blood volume. Radiology 254(1):1639
5. Barrett JF, Keat N (2004) Artifacts in CT: recognition and avoidance. Radiographics 24:1679–1691
6. Schindera ST, Tock I, Marin D, et al. (2010) Effect of beam hardening on arterial enhancement in thoracoabdominal CT angiography with increasing patient size: an in vitro and in vivo study. Radiology 256:528–535
7. Campbell SG, Croskerry P, Bond WF (2007) Profiles in patient safety: a ''perfect storm'' in the emergency department. Acad Emerg Med 14:743–749
8. Pinto A, Reginelli A, Pinto F, et al. (2016) Errors in imaging patients in the emergency setting. Br J Radiol 89(1061):20150914
9. Marin D, Boll DT, Mileto A, Nelson RC (2014) State of the art: dual-energy CT of the abdomen. Radiology 271(2):327–342
10. Megibow AJ, Sahani D (2012) Best practice: implementation and use of abdominal dual-energy CT in routine patient care. AJR Am J Roentgenol 199(5 Suppl):S71–S77
11. Grajo JR, Patino M, Prochowski A, Sahani DV (2016) Dual energy CT in practice: basic principles and applications. Appl Radiol 45:6–12
12. McCollough CH, Leng S, Yu L, Fletcher JG (2015) Dual- and multienergy CT: principles, technical approaches, and clinical applications. Radiology 276(3):637–653
13. Shuman WP, O'Malley RB, Busey JM, Ramos MM, Koprowicz KM (2017) Prospective comparison of dual-energy CT aortography using 70% reduced iodine dose versus single-energy CT aortography using standard iodine dose in the same patient. Abdom Radiol (NY) 42(3):759–765
14. Kaza RK, Ananthakrishnan L, Kambadakone A, Platt JF (2017) Update of dual-energy CT applications in the genitourinary tract. AJR Am J Roentgenol 208(6):1185–1192
15. Postma AA, Das M, Stadler AA, Wildberger JE (2015) Dual-Energy CT: what the neuroradiologist should know. Curr Radiol Rep 3:16
16. Kalisz K, Halliburton S, Abbara S, et al. (2017) Update on cardiovascular applications of multienergy CT. Radiographics 37(7):1955–1974
17. Goldman LW (2008) Principles of CT: multislice CT. J Nucl Med Technol 36:57–68
18. Almeida IP, Schyns LE, Öllers MC, et al. (2017) Dual-energy CT quantitative imaging: a comparison study between twin-beam and dual-source CT scanners. Med Phys 44(1):171–179
19. Wang L, Liu B, Wu XW, et al. (2012) Correlation between CT attenuation value and iodine concentration in vitro: discrepancy between gemstone spectral imaging on single-source dual-energy CT and traditional polychromatic X-ray imaging. J Med Imaging Radiat Oncol 56:379–383
20. Matsuda I, Akahane M, Sato J, et al. (2012) Precision of the measurement of CT numbers: comparison of dual-energy CT spectral imaging with fast kVp switching and conventional CT with phantoms. Jpn J Radiol 30:34–39
21. Coursey CA, Nelson RC, Boll DT, et al. (2010) Dual-energy multidetector CT: how does it work, what can it tell us, and when can we use it in abdominopelvic imaging? Radiographics 30(4):1037–1055
22. Patino M, Prochowski A, Agrawal MD, et al. (2016) Material separation using dual-energy CT: current and emerging applications. Radiographics 33(4):1087–1105
23. Sellerer T, Noël PB, Patino M, et al. (2018) Dual-energy CT: a phantom comparison of different platforms for abdominal imaging. Eur Radiol 7:2745–2755
24. Im AL, Lee YH, Bang DH, Yoon KH, Park SH (2013) Dual energy CT in patients with acute abdomen; is it possible for virtual non-enhanced images to replace true non-enhanced images? Emerg Radiol 20:475–483
25. Borhani AA, Kulzer M, Iranpour N, et al. (2017) Comparison of true unenhanced and virtual unenhanced (VUE) attenuation values in abdominopelvic single-source rapid kilovoltage-switching spectral CT. Abdom Radiol 42:710–717
26. Zhao YE, Wang ZJ, Zhou CS (2014) Multidetector computed tomography of superior mesenteric artery: anatomy and pathologies. Can Assoc Radiol J. 65:267–274
27. Cordeiro MA, Lima JA (2006) Atherosclerotic plaque characterization by multidetector row computed tomography angiography. J Am Coll Cardiol 47(8 Suppl):C40–C47
28. Harnik IG, Brandt LJ (2010) Mesenteric venous thrombosis. Vasc Med 15:407–418
29. Ascenti G, Sofia C, Mazziotti S, et al. (2016) Dual-energy CT with iodine quantification in distinguishing between bland and neoplastic portal vein thrombosis in patients with hepatocellular carcinoma. Clin Radiol. 71(9):938.e1–938.e9
30. Howard DP, Sideso E, Handa A, et al. (2014) Incidence, risk factors, outcome and projected future burden of acute aortic dissection. Ann Cardiothorac Sur. 3:278–284
31. Pinho DF, Kulkarni NM, Krishnaraj A, Kalva SP, Sahani DV (2013) Initial experience with single-source dual-energy CT abdominal angiography and comparison with single-energy CT angiography: image quality, enhancement, diagnosis and radiation dose. Eur Radiol 23(2):351–359
32. Vaidya S, Dighe M (2010) Spontaneous celiac artery dissection and its management. J Radiol Case Rep 4:30–33
33. Jesinger RA, Thoreson AA, Lamba R (2013) Abdominal and pelvic aneurysms and pseudoaneurysms: imaging review with clinical, radiologic, and treatment correlation. Radiographics 33:E71–E96
34. Wortman JR, Uyeda JW, Fulwadhva UP, Sodickson AD (2018) Dual-energy CT for abdominal and pelvic trauma. Radiographic 38(2):586–602
35. Machida H, Tanaka I, Fukui R, et al. (2016) Dual-energy spectral CT: various clinical vascular applications. Radiographics 36(4):1215–1232
36. Maturen KE, Kaza RK, Liu PS, et al. (2012) ''Sweet spot'' for endoleak detection: optimizing contrast to noise using low keV reconstructions from fast-switch kVp dual-energy CT. J Comput Assist Tomogr 36:83–87
37. Martin SS, Wichmann JL, Scholtz JE, et al. (2017) Noise-optimized virtual monoenergetic dual-energy CT improves diagnostic accuracy for the detection of active arterial bleeding of the abdomen. J Vasc Interv Radiol 28(9):1257–1266
38. Chandarana H, Godoy MC, Vlahos I, et al. (2008) Abdominal aorta: evaluation with dual-source dual-energy multidetector CT after endovascular repair of aneurysms—initial observations. Radiology 249:692–700
39. Buffa V, Solazzo A, D'Auria V, et al. (2014) Dual-source dual-energy CT: dose reduction after endovascular abdominal aortic aneurysm repair. Radiol Med 119(12):934–941
40. Flors L, Leiva-Salinas C, Norton PT, Patrie JT, Hagspiel KD (2013) Endoleak detection after endovascular repair of thoracic aortic aneurysm using dual-source dual-energy CT: suitable scanning protocols and potential radiation dose reduction. AJR Am J Roentgenol 200(2):451–460
41. Stolzmann P, Frauenfelder T, Pfammatter T, et al. (2008) Endoleaks after endovascular abdominal aortic aneurysm repair: detection with dual-energy dual-source CT. Radiology 249:682–691
42. Fujii T, Morita H, Sutoh T, et al. (2014) Arteriovenous malformation detected by small bowel endoscopy. Case Rep Gastroenterol 8(2):324–328
43. Dalle I, Geboes K (2002) Vascular lesions of the gastrointestinal tract. Acta Gastroenterol Belg 65(4):213–219
44. Makhoul F, Kaur P, Johnston TD, et al. (2008) Arteriovenous malformation of the pancreas: a case report and review of literature. Int J Angiol 17(4):211–213

45. Guo Y, Ou SX, Qian M, Zeng X, Li B (2015) Dual-energy CT angiography for the diagnosis of intracranial dural arteriovenous fistula. Int J Clin Exp Med 8(5):7802–7808
46. Postma AA, Hofman PA, Stadler AA, et al. (2012) Dual-energy CT of the brain and intracranial vessels. AJR Am J Roentgenol 199:S26–S33
47. Otrakji A, Digumarthy SR, Gullo RL, et al. (2016) Dual-energy CT: spectrum of thoracic abnormalities. Radiographics 36(1):38–52
48. Geffroy Y, Rodallec MH, Boulay-Coletta I, et al. (2011) Multidetector CT angiography in acute gastrointestinal bleeding: why, when, and how. Radiographics 31(3):E35–E46
49. Furlan A, Fakhran S, Federle MP (2009) Spontaneous abdominal hemorrhage: causes, CT findings, and clinical implications. AJR Am J Roentgenol 193(4):1077–1087
50. El-tawil AM (2012) Trends on gastrointestinal bleeding and mortality: where are we standing? World J Gastroenterol 18(11):1154–1158
51. Artigas JM, Martí M, Soto JA, et al. (2013) Multidetector CT angiography for acute gastrointestinal bleeding: technique and findings. Radiographics 33(5):1453–1470
52. Sin FN, Tsang JP, Siu KL, Ma JK, Yung AW (2012) Medications as causes of intraluminal hyperdensities: what radiologists need to know. Eur J Radiol 81(7):1652–1656
53. Sun H, Hou XY, Xue HD, et al. (2015) Dual-source dual-energy CT angiography with virtual non-enhanced images and iodine map for active gastrointestinal bleeding: image quality, radiation dose and diagnostic performance. Eur J Radiol 84(5):884–891
54. Lambert JW, FitzGerald PF, Edic PM, et al. (2017) The effect of patient diameter on the dual-energy ratio of selected contrast-producing elements. J Comput Assist Tomogr 41(3):505–510
55. Mongan J, Rathnayake S, Fu Y, et al. (2012) In vivo differentiation of complementary contrast media at dual-energy CT. Radiology 265(1):267–272
56. Wiesner W, Khurana B, Ji H, Ros PR (2003) CT of acute bowel ischemia. Radiology 226(3):635–650
57. Potretzke TA, Brace CL, Lubner MG, et al. (2015) Early small-bowel ischemia: dual-energy CT improves conspicuity compared with conventional CT in a swine model. Radiology 275(1):119–126
58. Fulwadhva UP, Wortman JR, Sodickson AD (2016) Use of dual-energy CT and iodine maps in evaluation of bowel disease. Radiographics. 36(2):393–406
59. Qiu D, Seeram E (2016) Does iterative reconstruction improve image quality and reduce dose in computed tomography? Radiol Open J 1(2):42–54
60. Willemink MJ, Schilham AM, Leiner T, et al. (2013) Iterative reconstruction does not substantially delay CT imaging in an emergency setting. Insights Imaging 4(3):391–397
61. Rassouli N, Etesami M, Azz Dhanantwari, et al. (2017) Detector-based spectral CT with a novel dual-layer technology: principles and applications. Insights Imaging 8(6):589–598
62. Aran S, Shaqdan KW, Abujudeh HH (2014) Dual-energy computed tomography (DECT) in emergency radiology: basic principles, techniques, and limitations. Emerg Radiol 21(4):391–405
63. Neogi T, Jansen TL, Dalbeth N (2015) 2015 gout classification criteria: an American College of Rheumatology/European League Against Rheumatism collaborative initiative. Arthritis Rheumatol 67(10):2557–2568
64. Andreucci M, Solomon R, Tasanarong A (2014) Side effects of radiographic contrast media: pathogenesis, risk factors, and prevention. Biomed Res Int . https://doi.org/10.1155/2014/741018
65. Xin L, Yang X, Huang N, et al. (2015) The initial experience of the upper abdominal CT angiography using low-concentration contrast medium on dual energy spectral CT. Abdom Imaging 40:2894–2899
66. Agrawal MD, Oliveira GR, Kalva SP, et al. (2016) Prospective comparison of reduced-iodine-dose virtual monochromatic imaging dataset from dual-energy CT angiography with standard-iodine-dose single-energy CT angiography for abdominal aortic aneurysm. AJR Am J Roentgenol 207(6):W125–W132
67. Uhrig M, Simons D, Kachelrieß M, et al. (2016) Advanced abdominal imaging with dual energy CT is feasible without increasing radiation dose. Cancer Imaging 16(1):15
68. Schick D, Pratap J (2016) Radiation dose efficiency of dual-energy CT benchmarked against single-source, kilovoltage-optimized scans. Br J Radiol 89(1058):20150486
69. Ho LM, Yoshizumi TT, Hurwitz LM, et al. (2009) Dual energy versus single energy MDCT: measurement of radiation dose using adult abdominal imaging protocols. Acad Radiol 16:1400–1407
70. De Cecco CN, Darnell A, Macias N, et al. (2013) Second-generation dual-energy computed tomography of the abdomen: radiation dose comparison with 64- and 128-row single-energy acquisition. J Comput Assist Tomogr 37:543–546
71. Parakh A, Macri F, Sahani D (2018) Dual-energy computed tomography: dose reduction, series reduction, and contrast load reduction in dual-energy computed tomography. Radiol Clin N Am 56(4):601–624
72. Ascenti G, Mazziotti S, Mileto A, et al. (2012) Dual-source dual-energy CT evaluation of complex cystic renal masses. AJR Am J Roentgenol 199(5):1026–1034
73. Dubourg B, Caudron J, Lestrat JP, et al. (2014) Single-source dual-energy CT angiography with reduced iodine load in patients referred for aortoiliofemoral evaluation before transcatheter aortic valve implantation: impact on image quality and radiation dose. Eur Radiol 24(11):2659–2668
74. Jepperson MA, Cernigliaro JG, el Ibrahim SH, et al. (2015) In vivo comparison of radiation exposure of dual-energy CT versus low-dose CT versus standard CT for imaging urinary calculi. J Endourol 29(2):141–146
75. Lin XZ, Wu ZY, Tao R, et al. (2012) Dual energy spectral CT imaging of insulinoma-value in preoperative diagnosis compared with conventional multi-detector CT. Eur J Radiol 81(10):2487–2494
76. Shuman WP, Green DE, Busey JM, et al. (2014) Dual-energy liver CT: effect of monochromatic imaging on lesion detection, conspicuity, and contrast-to-noise ratio of hypervascular lesions on late arterial phase. AJR Am J Roentgenol 203(3):601–606
77. Takeuchi M, Kawai T, Ito M, et al. (2012) Split-bolus CT-urography using dual-energy CT: feasibility, image quality and dose reduction. Eur J Radiol 81(11):3160–3165
78. American College of Radiology (2018) ACR-AAPM practice parameter for diagnostic reference levels and achievable doses in medical X-ray imaging. ACR website. https://www.acr.org/-/media/ACR/Files/Practice-Parameters/diag-ref-levels.pdf?la=en. Accessed 23 July 23 2018.
79. Wortman JR, Bunch PM, Fulwadhva UP, Bonci GA, Sodickson AD (2016) Dual-energy CT of incidental findings in the abdomen: can we reduce the need for follow-up imaging? AJR Am J Roentgenol 6:W1–W11
80. Deinzer CK, Danova D, Kleb B, et al. (2014) Influence of different iodinated contrast media on the induction of DNA double-strand breaks after in vitro X-ray irradiation. Contrast Media Mol Imaging 9(4):259–267